cite peer-reviewed, updated version:
Russell, R. P., Ocampo, C. A., "Geometric Analysis of Free-Return Trajectories Following a Gravity-Assisted Flyby," Journal of Spacecraft and Rockets, Vol. 42, No. 1, 2005, pp. 138-151.

A GEOMETRIC ANALYSIS OF HALF AND FULL-REVOLUTION RETURN TRAJECTORIES VIA PLANETARY FLYBYS*

Ryan P. Russell† and Cesar A. Ocampo‡
Department of Aerospace Engineering, The University of Texas at Austin
210 East 24th Street, W. R. Woolrich Laboratories
1 University Station, C0600
Austin, Texas 78712-1085

Given a spacecraft will flyby a planet with a specified hyperbolic energy, the purpose of this paper is to systematically identify all trajectories following the flyby that will directly return after the planet makes $n/2$ revolutions of the primary, where n is any positive integer. The method is geometric and uses solutions from Lambert's Problem when the transfer angle is $n\pi$. The resulting velocity diagram is a mission-planning tool with potential applications that include cycler trajectories and planetary moon tours. The generalized half and full-revolution free-return solutions may be used to construct loitering orbits about one celestial body or transfers between multiple bodies. Several previously documented cycler trajectories are improved using the discussed solutions.

NOMENCLATURE

Symbol	***Description***
a	semi-major axis
t	time
E	eccentric anomaly
F	focus of a transfer ellipse
M	number of complete revolutions made by the celestial body
N	number of complete revolutions made by the spacecraft
T	period
$\mathbf{r}$	position vector
$\mathbf{v}$	velocity vector
α, β, S	intermediate variables for Lambert's Equation
γ	flight path angle
μ	gravitational parameter of the primary
$\theta, \delta, r_1, r_2, c$	input geometry for Lambert's Equation, see Figure 2a

Subscript	***Description***
F	full-revolution return
H	half-revolution return
B	celestial body
o	initial
f	final
∞	relative to celestial body before or after flyby
v	vacant focus
r	radial component
θ	transverse component

* Presented as Paper AAS 03-508 at the AAS/AIAA Astrodynamics Specialists Meeting, Big Sky, Montana, August 2003.

† Ph.D. candidate. ryanrussell@mail.utexas.edu.
‡ Assistant Professor.

cite peer-reviewed, updated version:
Russell, R. P., Ocampo, C. A., "Geometric Analysis of Free-Return Trajectories Following a Gravity-Assisted Flyby," Journal of Spacecraft and Rockets, Vol. 42, No. 1, 2005, pp. 138-151.

INTRODUCTION

Free-return trajectories have been the subject of many studies in the wake and anticipation of taking humans back to the Moon and beyond.[1,2,3] Proven to be invaluable during the Apollo missions, free-returns are useful for human exploration because they return to the original body, by design or as an abort option, without any powered maneuvers. Free-returns are also useful on interplanetary missions or moon tours when consecutive flybys of the same body provide the appropriate timing and gravity-assisted maneuvers necessary to reach the next destination.

Half and full-rev free-returns, orbits with a transfer angle that is an odd or even integer multiple of π respectively, are subsets of the general free-return transfer. First termed by Hollister[4], half and full-rev returns were originally defined such that the spacecraft and the planet were limited to a 1π or 2π transfer respectively, and were used as stalling mechanisms in the construction of interplanetary cycler orbits. The half and full-rev returns are of particular interest because the solution space for the targeting problem significantly increases if the transfer angle is an integer multiple of π. The extra degrees of freedom subsets make it possible to find free-return solutions that are further constrained by the matching v_∞ conditions associated with gravity-assisted flybys. This concept has been applied to missions involving the Moon,[5,6] Jupiter,[7] Venus,[8] and Mars.[9,10,11]

In addition to generalizing the definitions for half and full-rev free-return trajectories to be odd and even $n\pi$ transfers, as done previously by Uphoff et al[7], the purpose of this paper is to express the solutions geometrically on a velocity diagram to provide a general design tool for multiple-flyby missions.

A geometric approach is used to find all feasible solutions on a velocity diagram that allow a spacecraft to enter a generalized full or half-rev free-return trajectory following an unpowered gravity-assisted flyby maneuver. The first section gives an overview of Lambert's multiple revolution problem in the context of $n\pi$ transfers. The second section outlines methods to obtain semi-major axis values for full and half-rev free-returns respectively. In the full-rev case, two methods are presented, a simple derivation based on orbital periods and a second more complete discussion based on Lambert's Equation. In the half-rev case, Lambert's Equation is used exclusively. The third section discusses the terminal velocity vectors that initiate full and half-rev free-returns, and expresses the solutions on a common flyby velocity diagram. The final two sections include an example application that uses $n\pi$ transfers to find several promising Earth-Mars cyclers, followed by a discussion of conclusions and anticipated work.

LAMBERT'S PROBLEM

Half and full-rev returns are specific cases of the classic Lambert targeting problem when the transfer angle is an integer multiple of π and 2π respectively. It is well known that these cases lead to singularities when computing terminal velocity vectors using standard approaches. In order to understand the behavior of the solutions at these singularities, it is useful to look at them in the limit as they approach half and full-rev returns. This section gives an introduction to Lambert's problem in general[12] and in the context of $n\pi$ transfers. The following sections will examine the application of Lambert's equation to half and full-rev returns in more detail.

The sum of the two chords connecting any point on a given ellipse to its two respective foci is a constant. From this familiar "tac and string" property, a diagram similar to that in Figure 1a can be drawn to find all vacant foci locations for elliptic transfers from $\mathbf{r_1}$ to $\mathbf{r_2}$ given any sufficiently large value for semi-major axis.

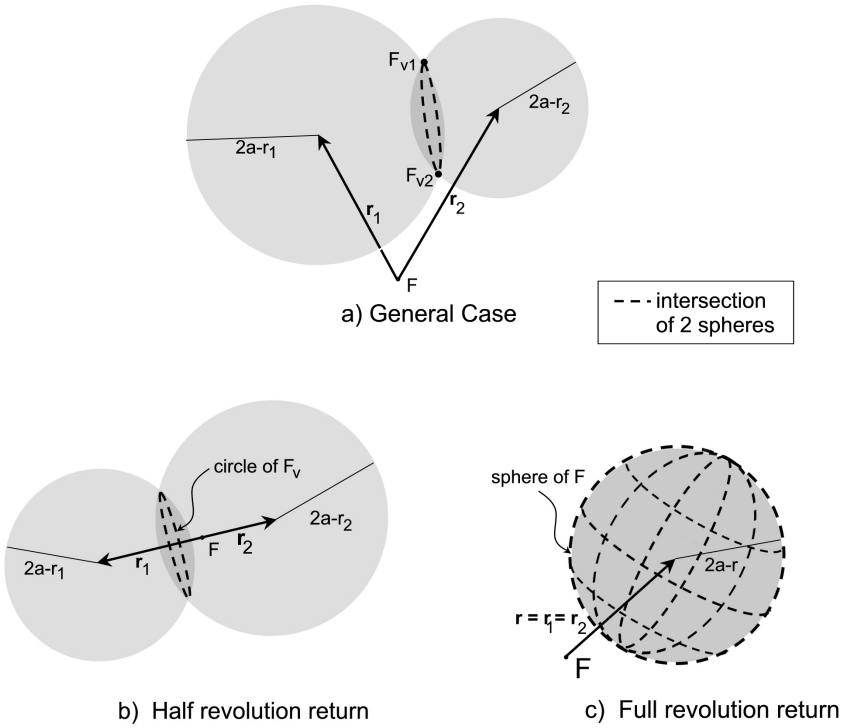

Figure 1: Procedure to find vacant foci

The spheres centered at the tips of $\mathbf{r_1}$ and $\mathbf{r_2}$ are the locus of all vacant foci for ellipses of semi-major axis *a,* that contain the position vectors $\mathbf{r_1}$ and $\mathbf{r_2}$, respectively. The intersection of the two spheres is illustrated with a dotted circle in parts a and b. Note, in part c, the intersection is a sphere rather than a circle. In the general case, if $\mathbf{r_1}$ is not parallel to $\mathbf{r_2}$, then the transfer plane is defined by the two position vectors. The intersection of this transfer plane and the dotted circle are the two points labeled as F_{v1} and F_{v2}. These are the two vacant foci locations for elliptic transfers from $\mathbf{r_1}$ to $\mathbf{r_2}$ with semi-major axis *a*. However, if the transfer angle is $(2N+1)\pi$, as is true for a half-rev return, then the transfer plane is no longer defined by the position vectors, and any point on the dotted circle on Figure 1b is a valid location for the vacant focus. The same is true if the transfer angle is $2N\pi$ and $\mathbf{r_1} \neq \mathbf{r_2}$. If the transfer angle is $2N\pi$ and $\mathbf{r_1} = \mathbf{r_2}$, as is true for a full-rev return, then the two spheres collapse into one. Thus, from Figure 1c, any location on the sphere of radius $2a-r$ is a valid location for a vacant focus. In summary, there are only two vacant foci locations in the general case, one degree of freedom is required to specify the location for a half-rev return (and also when $\mathbf{r_1} \neq \mathbf{r_2}$ and the transfer angle is $2N\pi$), and lastly, two degrees of freedom are required to specify the vacant focus location for a full-rev return.

Figure 2a shows the four transfers on the two possible ellipses in the general case. Figure 2b and Figure 2c illustrate the transfers in the limit as they approach a half and full-rev return respectively. Note, the angle, $\theta - 2N\pi$, is defined to always be less than or equal to π. Therefore, $\delta - 2N\pi$ is always defined to be greater than or equal to π.

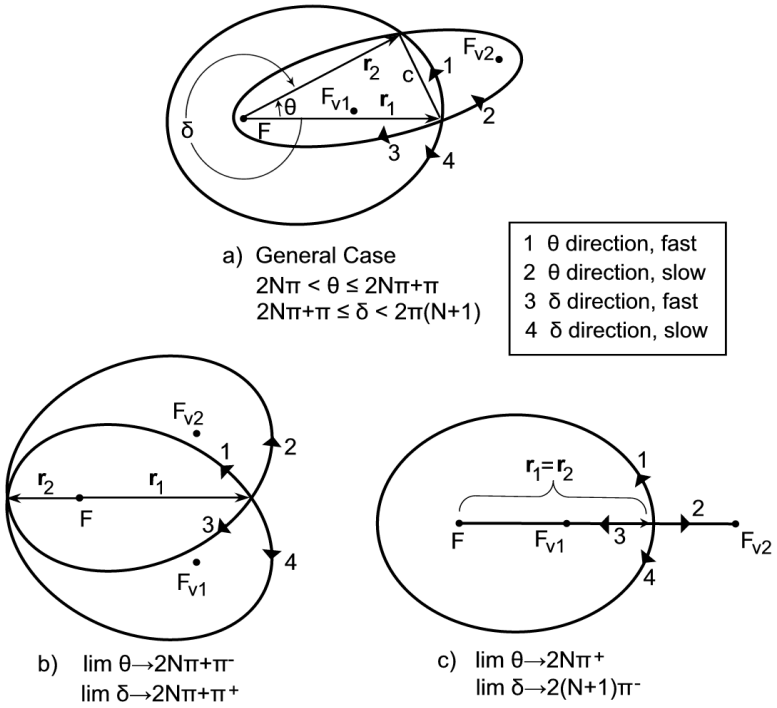

Figure 2: The four possible arcs of Lambert's Equation for a given *N*

Lambert's theorem states that the time of flight connecting any two points on an elliptic orbit is a function only of its semi-major axis, the chord length between the two points, and the sum of the respective distances from the focus to the two points. Eq. (1) summarizes the Lagrangian formulation generalized to include multiple revolutions of the primary as defined in Figure 2a. Eq. (1) holds true for all four transfers shown in Figure 2. The quadrant ambiguities associated with the angles α and β uniquely characterize each of the four arcs. The solution associated with $\alpha = \alpha_0$ is termed "fast" while the solution associated with $\alpha = 2\pi - \alpha_0$ is termed "slow," indicating a slow solution has a longer time of flight than a fast solution given two transfers with a common semi-major axis.

$$\sqrt{\mu}\ TOF = a^{3/2}\left[2N\pi + \alpha_{fast,slow} - \beta - \sin(\alpha_{fast,slow}) + \sin(\beta)\right] \tag{1}$$

where,

$$\sin\left(\alpha_0/2\right) = \sqrt{S/(2a)}$$

$$\alpha_{fast} = \alpha_0$$

$$\alpha_{slow} = 2\pi - \alpha_0$$

$$\sin\left(\beta_0/2\right) = \sqrt{(S-c)/(2a)}$$

$$\beta = \beta_0 \quad \text{if transfer angle is } \theta$$

$$\beta = -\beta_0 \quad \text{if transfer angle is } \delta$$

$$S = 1/2\left(r_1 + r_2 + c\right)$$

GENERALIZED FULL-REVOLUTION RETURN SOLUTIONS

The generalized full-rev return is defined to be any trajectory that leaves a celestial body and returns directly to the same body after completing N revolutions of the primary while the celestial body completes M revolutions. Because the times of flight for full-rev returns are simple integer multiples of a celestial body's period, the governing equation of full-rev returns, Eq. (2), is derived by setting the times of flight for both the spacecraft and the celestial body to be equal.

$$M\left[2\pi\sqrt{a_B{}^3/\mu}\right] = N\left[2\pi\sqrt{a_F{}^3/\mu}\right] \tag{2}$$

Solving for a_F, the expression for the semi-major axis of a full-rev transfer becomes,

$$a_F = a_B\left(M/N\right)^{2/3} \tag{3}$$

Additional Insight from Lambert's Equation

Eq. (2) can also be derived directly from Lambert's Equation. The first step in deriving Eq. (1), shown in Eq. (4), is to subtract Kepler's Equation applied to $\mathbf{r_1}$ from Kepler's Equation applied to $\mathbf{r_2}$. The angles α and β are alternate parameters that can be shown to be functions of E_1 and E_2.

$$\sqrt{\mu}\ TOF = a^{3/2}\left[E_2 - E_1 - \sin(E_2) + \sin(E_1)\right] \tag{4}$$

When $\mathbf{r_2} = \mathbf{r_1}$, and consequently $E_2 = E_1 + 2N\pi$, it becomes,

$$\sqrt{\mu}\ TOF = a^{3/2}\left[2N\pi\right] \tag{5}$$

Eq. (5) is identical to Eq. (2) when $a=a_F$ and TOF is constrained to be M times the period of the celestial body.

The general form of Lambert's Equation gives additional insight to the problem when observing the solutions in the limit as $\mathbf{r}_1 \rightarrow \mathbf{r}_2$. Examining Figure 2a, as $\mathbf{r}_1 \rightarrow \mathbf{r}_2$ and consequently $\theta \rightarrow 2N\pi^+$ and $\delta \rightarrow 2(N+1)\pi^-$, the attracting focus, the tip of the position vectors, and the two empty foci become collinear as seen in Figure 2c. The only possible ellipse with a position vector directly between foci F and F_{v2} is a rectilinear ellipse with e=1. The only possible ellipse with foci F and F_{v1} that contains $\mathbf{r}$ is one whose apoapse occurs at $\mathbf{r}$, thus e=1-r/a. Both solutions are shown in Figure 2c. In the limit, the two position vectors are very close, but never exactly parallel, thus a transfer plane is defined, and the two vacant foci are unique, as illustrated in Figure 2a. The transfers approach those illustrated in Figure 2c, and properties of the solutions smoothly approach values as outlined in Table 1. However, when $\mathbf{r}_1 = \mathbf{r}_2$ exactly, the transfer plane is no longer defined, and the vacant focus can be anywhere on the sphere of possible locations, as seen in Figure 1c. Thus, the rectilinear ellipse and the non-rectilinear ellipse in Figure 2c represent just two points on the vacant foci sphere. Transfers 1 and 4 are specific cases of the solutions described by Eq. (2). However, transfers 2 and 3 are not described by Eq. (2) because the eccentric anomalies at the beginning and end of the transfers are different. Examining Figure 2a, as $\mathbf{r}_1 \rightarrow \mathbf{r}_2$, it is apparent that $E_o \rightarrow E_f$ for transfers 1 and 4, but not for transfers 2 and 3. Expressions for these values, as well as other noteworthy properties for each of the four transfers, are given in Table 1.

Table 1: Properties of Lambert solutions in the limit as $\mathbf{r}_1 \rightarrow \mathbf{r}_2$ $[\theta \rightarrow 2N\pi^+, \delta \rightarrow 2(N+1)\pi^-]$

	transfer 1	transfer 2	transfer 3	transfer 4
transfer angle	$\theta \rightarrow 2N\pi^+$	$\theta \rightarrow 2N\pi^+$	$\delta \rightarrow 2(N+1)\pi^-$	$\delta \rightarrow 2(N+1)\pi^-$
transfer ellipse period	T	T	T	T
time of flight	$N\,T$	$N\,T + \Delta t$	$(N+1)\,T - \Delta t$	$(N+1)\,T$
e	r/a-1	1	1	r/a-1
initial E	π^-	E_0	$2\pi - E_0$	π^+
final E	π^+	$2\pi - E_0$	E_0	π^-

where $E_0 = \pi - \cos^{-1}\left[\left(r-a\right)/a\right]$, $\Delta t = 2\pi - 4\sin^{-1}\left(\sqrt{r/(2a)}\right) + 2\sqrt{2ar - r^2}/a$, and $T = 2\pi\sqrt{a^3/\mu}$

Every point on the vacant foci sphere has a direct and retrograde transfer, each with a time of flight equal to $2N\pi$ TU. However, the point on the sphere that is exterior to and collinear with F and **r** has two additional transfers because its associated ellipse is rectilinear. Eq. (2) covers all the solutions such that $E_o = E_f$, including two of the four possible transfers on the rectilinear ellipse. The remaining two solutions on the rectilinear ellipse are transfers 2 and 3 as shown in Figure 2c where $E_o \neq E_f$. For a given value of M and N, the two transfers on each ellipse associated with every point on the vacant foci sphere in addition to the two rectilinear solutions such that $E_o \neq E_f$ comprise the set of all even $n\pi$ transfers with a common semi-major axis.

In the limiting case when $\mathbf{r}_1=\mathbf{r}_2$, then $c=0$, $\alpha_0=\beta_0$, and Eq. (1) simplifies to Eqs. (6), (7), (8), and (9) respectively for transfers 1, 2, 3, and 4 shown in at Figure 2c.

$$\sqrt{\mu}\ TOF = a^{3/2} 2N\pi \tag{6}$$

$$\sqrt{\mu}\ TOF = a^{3/2}\left[2\pi\left(N+1\right) - 4\sin^{-1}\left(\sqrt{r/(2a)}\right) + 2\sqrt{2ar-r^2}\,/a\right] \tag{7}$$

$$\sqrt{\mu}\ TOF = a^{3/2}\left[2N\pi + 4\sin^{-1}\left(\sqrt{r/(2a)}\right) - 2\sqrt{2ar-r^2}\,/a\right] \tag{8}$$

$$\sqrt{\mu}\ TOF = a^{3/2} 2\pi\left(N+1\right) \tag{9}$$

Eqs. (6) and (9) are identical to Eq. (5) except the N is phased by one in Eq. (9) because the transfer angle is δ rather than θ. As an example, suppose it is desirable to traverse one revolution of the primary. If transfer 1 is used, the associated N is one because the transfer angle, θ, approaches $2\pi^+$, and a full revolution is completed as $\mathbf{r}_1 \rightarrow \mathbf{r}_2$. However, if transfer 4 is used, the associated N is zero because the transfer angle, δ, approaches $2\pi^-$, and a full revolution is not reached as $\mathbf{r}_1 \rightarrow \mathbf{r}_2$.

Figure 3 and Figure 4 plot the four time of flight vs. semi-major axis curves expressed in Eqs. (6)-(9) representing all four full-rev transfer arcs. The plots were generated using canonical variables with μ=1 AU^3/TU^2, r=1 AU, and N=0→5. Figure 5 is the two prior figures plotted on the same axes. Note that the transfer 1 curve is identical to the transfer 4 curve when N is phased by one, as evidenced from Eqs. (6) and (9). Also, the values of the $TOF(a_{min})$ and $\partial TOF/\partial a(a_{min})$ are equal for the transfer 2 and 3 curves when N is phased by one. This is easily shown using Eqs. (7) and (8) and recognizing that $a_{min}=S/2$.

Figure 5 contains all time of flight and semi-major axis information for transfers that make $2N\pi$ revolutions of the primary. More information is necessary to pick out the specific transfers that leave and return to a particular celestial body. Clearly, the trajectory of the celestial body must also lie on one of the curves in Figure 5. Since a rectilinear ellipse is not a physically realistic solution, the trajectory of the body can only be a transfer 1 or transfer 4 curve. A vertical dotted line is drawn at $a=a_B$. An example value of a_B=1 AU is used in the figures. The intersections of this vertical line with the transfer 1 and 4 curves locate the solutions that correspond to the trajectory of the celestial body. The horizontal dotted lines are then drawn at each of the intersections. Each integer multiple of the celestial body's period is associated with a horizontal dotted line, corresponding to values of M in Eq. (2). Finally, the intersections of the transfer lines with these horizontal lines represent specific semi-major axis values that will yield orbits that return to the body after N revolutions.

For example, there are five values of semi-major axis that yield non-rectilinear orbits that return after the celestial body makes two complete revolutions of the primary. Examining Figure 5, the five values for semi-major axis are found by locating the intersections of the top horizontal dotted line with the transfer 1 and 4 curves. The values are identical to those obtained with Eq. (3).

cite peer-reviewed, updated version:
Russell, R. P., Ocampo, C. A., "Geometric Analysis of Free-Return Trajectories Following a Gravity-Assisted Flyby," Journal of Spacecraft and Rockets, Vol. 42, No. 1, 2005, pp. 138-151.

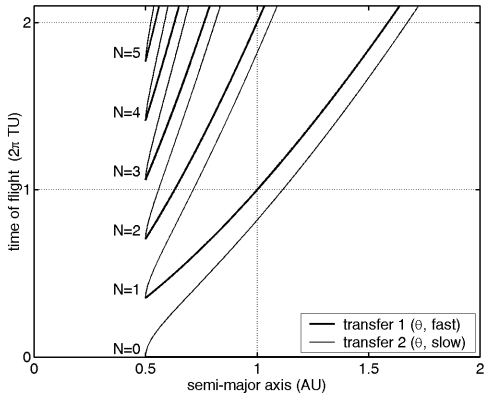

Figure 3: Limit $r_1 \rightarrow r_2$, Lambert solutions 1, 2

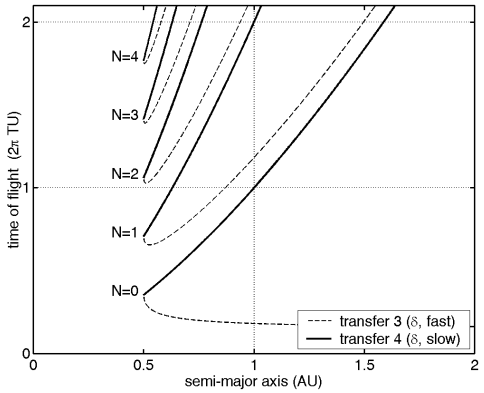

Figure 4: Limit $r_1 \rightarrow r_2$, Lambert solutions 3, 4

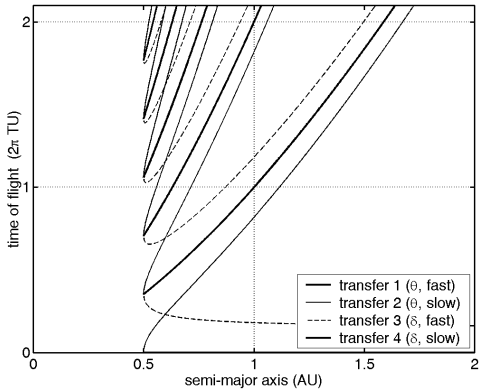

Figure 5: Limit $r_1 \rightarrow r_2$, Lambert solutions 1-4

GENERALIZED HALF-REVOLUTION RETURN SOLUTIONS

The generalized half-rev return is any trajectory that leaves a celestial body and returns directly to the same body after completing N+1/2 revolutions of the primary. When N=0, the half-rev return is also known as a backflip[6] trajectory. Examining Figure 1b, when the transfer angle is $2N\pi+\pi$, any point on the dotted circle is a valid location for the vacant focus. The alternate focus locations represent a rotation of the transfer orbit about the position vectors. Thus, the shape of the transfer ellipse is fixed, but a free parameter is required to specify the transfer plane.

A simple expression similar to Eq. (2) is not available for the half-rev return because the times of flight are not simple multiples of the orbital periods. Lambert's Equation is necessary for the analysis. In the limit as the transfer angle approaches $2N\pi+\pi$, as seen in Figure 2b, the first and second Lambert transfers become mirror images of the third and fourth respectively. Similar to the full-rev discussion, the two vacant foci of the ellipses in Figure 2b correspond to specific opposing locations on the dotted circle in Figure 1b.

$$\sqrt{\mu}\ TOF = a^{3/2}\left[2N\pi + 2\sin^{-1}\left(\sqrt{(r_1+r_2)/2a}\right) - \sqrt{\left(2a-r_1-r_2\right)\left(r_1+r_2\right)}\Big/a\right] \tag{10}$$

$$\sqrt{\mu}\ TOF = a^{3/2}\left[2\pi\left(N+1\right) - 2\sin^{-1}\left(\sqrt{(r_1+r_2)/2a}\right) + \sqrt{\left(2a-r_1-r_2\right)\left(r_1+r_2\right)}\Big/a\right] \tag{11}$$

Eq. (1) simplifies to Eq. (10) for transfers 1 and 3, and simplifies to Eq. (11) for transfers 2 and 4. The solution is indifferent to using the δ or θ direction because $\beta_0 = -\beta_0 = 0$ in Eq. (1). Figure 6 shows the time of flight vs. semi-major axis plots for a sample half-rev geometry using μ=1 AU^3/TU^2, $r_1 = r_2 = a_B = 1$ AU, and N=0 →5. In canonical terms, one revolution for the celestial body is 2π TU. Thus, the vertical axis is labeled in celestial body periods. In Figure 6, the semi-major axes that correspond to half-rev solutions are denoted by the intersections of the dotted lines and the transfer curves. Note that $r_1 = r_2$, $a_B = a_{min}$, and the horizontal lines occur exactly at half periods, indicating the celestial body is in a circular orbit. As an example, if a spacecraft leaves a celestial body at $\mathbf{r}_1$ and the time of flight is 4.5 celestial body periods, then there are nine semi-major axis values that yield transfers that will re-encounter the body at $\mathbf{r}_2$. The two solutions from N=4 are more easily seen in Figure 7.

For the special case of $a_B > a_{min}$ and $r_1 = r_2$, the celestial body must be in an elliptic orbit with its line of apses perpendicular to the terminal position vectors. In this case, the vertical dotted line corresponding to a_B should be moved accordingly in Figure 6 and the procedure to find the half-rev solutions is similar to that described below when $r_1 \neq r_2$.

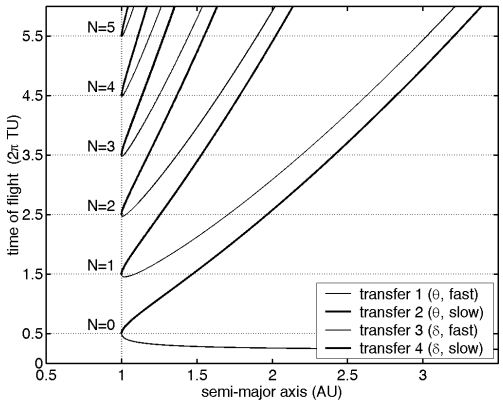

Figure 6: Half-rev solutions, $|\mathbf{r}_1|=|\mathbf{r}_2|$

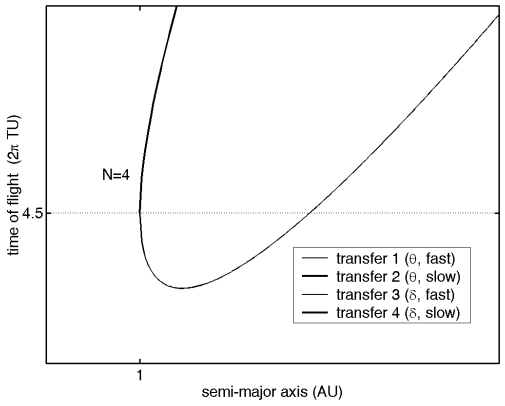

Figure 7: Zoom view of the *N*=4 curve

Figure 8 represents the more general case where $r_1 \neq r_2$. For this example, r_2=0.45 AU and the other parameters remain unchanged. Before identifying solutions that return to the body, it is necessary to specify whether the body is on a fast or slow path solution. If the body is on a fast path, then the times of flight corresponding to half-rev returns are denoted by the intersections of the vertical dotted line, positioned at $a=a_B$, with the fast transfer curves. These intersections are marked with horizontal dashed lines, each with an associated value of M that increases with TOF. If the body is on a slow path, the horizontal dotted curves indicate the half-rev return times of flight. Notice that successive dashed and dotted lines are respectively spaced by the period of the celestial body. The bottom dashed and dotted lines correspond to the M=0 fast and slow path solutions respectively.

cite peer-reviewed, updated version:
Russell, R. P., Ocampo, C. A., "Geometric Analysis of Free-Return Trajectories Following a Gravity-Assisted Flyby," Journal of Spacecraft and Rockets, Vol. 42, No. 1, 2005, pp. 138-151.

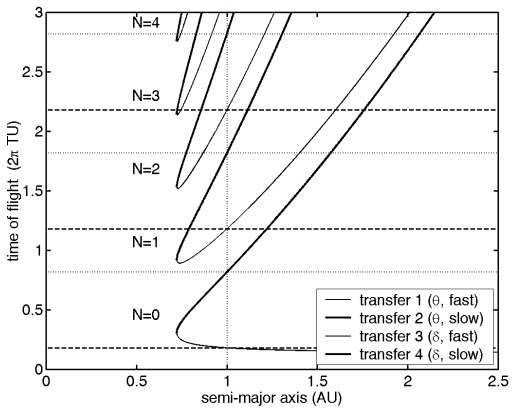

Figure 8: Half-rev solutions, $|\mathbf{r}_1| \neq |\mathbf{r}_2|$

For example, from Figure 8, suppose the celestial body with a_B=1 is on a fast path transfer, then there are seven M=2 solutions that return to the body. The M=2 solutions are marked by the dashed line with TOF=2.18 x 2π TU. The two N=3 intersections occur at a=0.73 and a= 0.75 AU. The two N=2 intersections occur at a=0.86 and a= 1 AU. Note the latter corresponds to the path of the celestial body. The two N=1 intersections occur at a=1.11 and a= 1.60 AU. Lastly, the one N=0 intersection occurs at a=1.76 AU.

FLYBY VELOCITY DIAGRAMS

The previous two sections provide methods to obtain semi-major axis values for full and half-rev solutions respectively. Based on these values, this section discusses the outbound velocity vectors required to initiate full and half-rev free-returns, and expresses the solutions on three-dimensional velocity diagrams.

Full-revolution Velocity Diagrams

If a spacecraft leaves a celestial body on an orbit with the semi-major axis a_F, obtained from Eq. (3) or a plot similar to Figure 5, then it will return directly after it completes N revolutions. Eq. (12) is the Vis-viva Equation solved for spacecraft velocity magnitude. Inserting Eq. (3) into Eq. (12) gives Eq. (13), and restates the constraint in terms of velocity magnitude.

$$v_F = \sqrt{2\mu/r - \mu/a_F} \tag{12}$$

$$v_F = \sqrt{2\mu/r - \mu\left(N/M\right)^{2/3}/a_B} \tag{13}$$

If a spacecraft leaves a celestial body with the speed relative to the primary given by Eq. (13), then it will return after it completes N revolutions. The constraints described in Eqs. (3) and (13) are identical to the constraint that the absent focus must lie on the sphere of intersection from Figure 1c. The scalar nature of Eq. (13) is significant because the direction of the velocity magnitude is unconstrained. This provides a convenient method to parameterize the two degrees of freedom associated with full-rev returns. Feasible values for N, M, r, μ, and a_B are combinations such that v_F from Eq. (13) is non-imaginary. For fixed values of M, r, μ, and a_B, N can vary from 1 to N_{max}.

If a celestial body with semi-major axis a_B is located a distance r from the primary, then for a given M and N, the locus of all spacecraft velocity vector tips that initiate full-rev returns is a sphere. The full-rev sphere is centered at the base of the body's velocity and has a radius of v_F. If a spacecraft approaches a body with an arbitrary hyperbolic speed and direction, the locus of all feasible points for the velocity after an unpowered gravity-assisted flyby is the surface of a sphere with radius v_∞ centered at the

tip of the body's velocity. This is the common three-dimensional velocity diagram for a gravity-assisted maneuver. A sample diagram with these spheres is illustrated in Figure 9. Canonical units were used to generate the figure with μ=1 AU^3/TU^2, $r = a_B$ =1 AU, N = 7, M= 4, and v_∞= 0.5 AU/TU. The right-handed coordinate system chosen for illustration and analysis of these diagrams is centered at the v_∞ sphere with the z axis aligned with $\mathbf{v}_B$ and the y axis opposed to the celestial body's angular momentum vector. The sphere centered at the base of $\mathbf{v}_B$ is the full-rev sphere associated with Eq. (13). The sphere centered at the tip of $\mathbf{v}_B$ the v_∞ sphere. The circle marks the intersection of the two spheres. If $\mathbf{v}_{\infty+}$ is located anywhere on this circle, the spacecraft and body will re-encounter after completing seven and four revolutions respectively. Figure 10 illustrates all of the full-rev spheres associated with M=4. It is clear that nine of the full-rev spheres intersect with the v_∞ sphere to form full-rev circles. If $\mathbf{v}_{\infty+}$ is located on any of the full-rev circles illustrated in Figure 10, then the spacecraft and body will re-encounter after the body completes four revolutions. N_{max} is eleven in this example. However, all eleven spheres do not necessarily intersect with the v_∞ sphere. Eq. (14) is a logical expression that must be true for an intersection to exist for a given v_B, v_F, and v_∞.

$$\left\{v_F \geq \left|v_B - v_\infty\right|\right\} \text{and} \left\{v_F \leq v_B + v_\infty\right\} \tag{14}$$

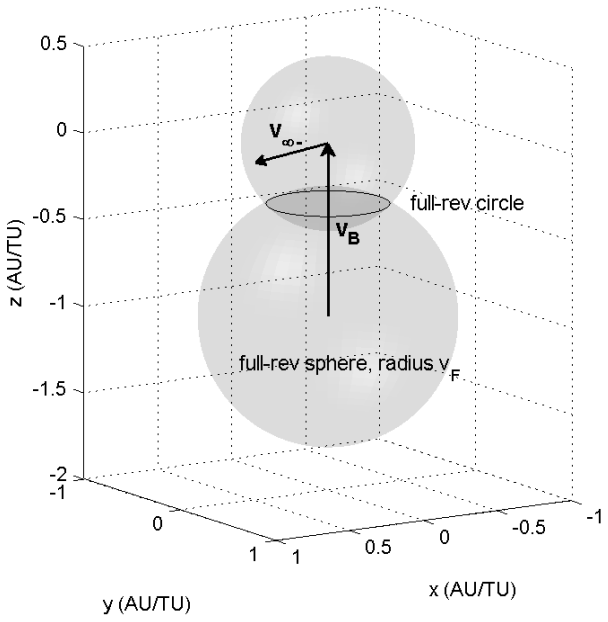

Figure 9: Full-rev velocity diagram, N=7, M=4

cite peer-reviewed, updated version:
Russell, R. P., Ocampo, C. A., "Geometric Analysis of Free-Return Trajectories Following a Gravity-Assisted Flyby," Journal of Spacecraft and Rockets, Vol. 42, No. 1, 2005, pp. 138-151.

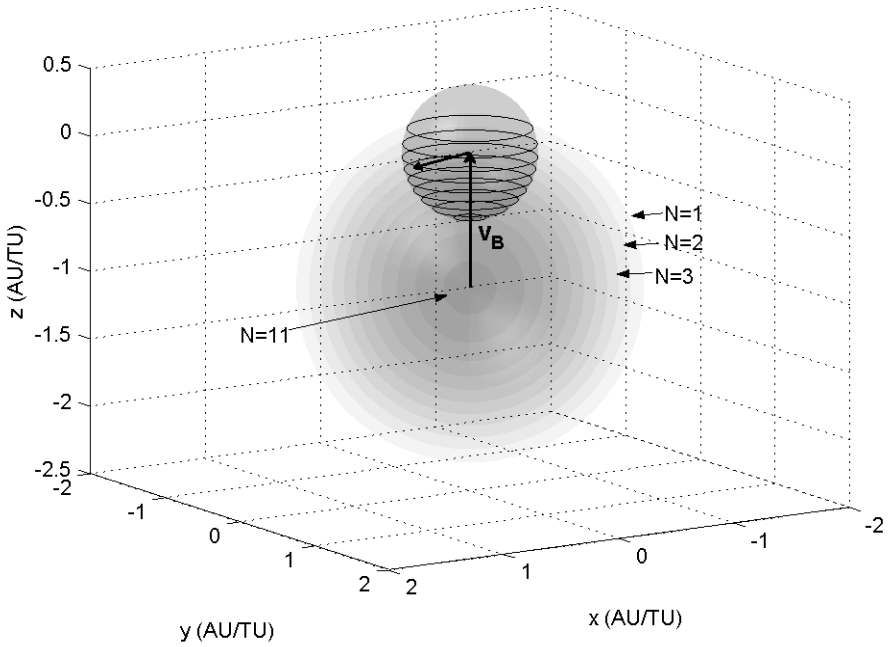

Figure 10: Full-rev velocity diagram, *N*=1→11, *M*=4

The equation describing the surface of the v_∞ and v_F spheres are given by Eqs. (15) and (16).

$$x^2 + y^2 + z^2 = v_\infty^2 \tag{15}$$

$$x^2 + y^2 + \left(z + v_B\right)^2 = v_F^2 \tag{16}$$

Eliminating *x* and *y*, Eq. (17) gives the z value for the full-rev circle of intersection.

$$z_F = \left(v_F^2 - v_\infty^2 - v_B^2\right) \Big/ 2v_B \tag{17}$$

Half-revolution Velocity Diagrams

The *f* and *g* functions are typically used to solve for the terminal velocity vectors on a transfer with a known value for semi-major axis. However, singularities exist in these functions when the transfer angle is an integer multiple of π. For full-rev returns, it was determined that the terminal velocity vectors can be located anywhere on a sphere with radius given in Eq. (13). For a half-rev return, the components of the outbound terminal velocity vector are derived by Battin[13] and expressed in Eqs. (18) and (19).

$$v_{Hr}^2 = \mu\left[2/(r_1 + r_2) - 1/a\right] \tag{18}$$

$$v_{H\theta}^2 = 2\mu r_2 \Big/ (r^2{}_1 + r_1 r_2) \tag{19}$$

Figure 11 is a diagram of the velocity vector, $\mathbf{v}_H$, in the ecliptic plane that produces a half-rev return orbit. The *x* axis of the primed coordinate system is aligned with $\mathbf{r}_B$ while the unprimed *z* axis is aligned with $\mathbf{v}_B$. Because the transfer plane is not specified, $\mathbf{v}_H$ can be rotated by any angle about $\mathbf{r}_B$ and the resulting velocity vector will initiate a half-rev return. Notice the squares in the component equations indicate double valued solutions. If the solution is a fast transfer, then it initially moves toward periapse, thus the radial component of the velocity that initiates the return must be negative. The opposite is true for a slow transfer. Examining Figure 2b, it is clear that the two fast transfers, 1 and 3, have negative initial radial components for velocity. It is also clear that the two slow transfers, 2 and 4, initially move toward apoapse and have positive initial radial components of velocity. For the transverse component, the positive

and negatives values produce half-rev returns because the transfer plane is undefined. The positive value, however, is used to reference the zero-point for the free angle that specifies the transfer plane.

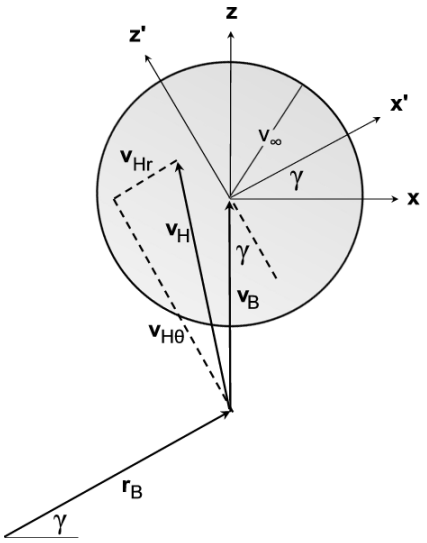

Figure 11: Outbound velocity components for half-rev free-returns

Examining Figure 11, the rotation of $\mathbf{v}_H$ about $\mathbf{r}_B$ forms a cone. The base of this cone, the half-rev circle, is the locus of all terminal velocity vector tips that lead to a half-rev return with a given semi-major axis. Uphoff and Crouch[6] refer to this cone as the equal gamma cone.

Figure 12 is an example velocity diagram that contains a half-rev circle. Generated using information from Figure 6, it includes $\mathbf{v}_{\infty -}$, $\mathbf{v}_B$, the v_∞ sphere, and the half-rev circle that corresponds to the slow N=2 solution with a time of flight of 3.5 celestial body periods. The slow N=2 curve from Figure 6 has a semi-major axis of 1.18 when the time of flight is 3.5 periods. Inserting this into Eqs. (18) and (19) gives v_{Hr}=0.153 and $v_{H\theta}$=1. Because a=1.18 is a slow solution, meaning it comes from the upper of the two N=2 curves, v_{Hr} must be positive.

In general, the plane of any half-rev circle is perpendicular to $\mathbf{r}_B$. Particular to this example, the plane of the half-rev circle in Figure 12 is the y-z plane because the celestial body is in a circular orbit. It is clear from Figure 11, that the directions of v_{Hr} and $v_{H\theta}$ are aligned with the x and z axes respectively when the flight path angle is zero.

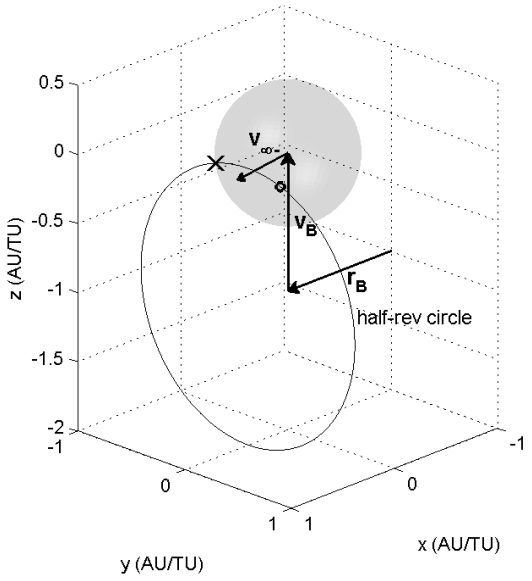

Figure 12: Half-rev velocity diagram, *M*=3.5, *N*=2 slow

The v_∞ sphere and the half-rev circle intersect at two locations, one below and one above the ecliptic plane, or the *x*-*z* plane. They are marked with an 'x' and 'o' respectively. These are the two feasible locations for $\mathbf{v}_{\infty+}$ following an un-powered flyby that will initiate this particular half-rev return. From Figure 11, in terms of the primed coordinates, the expressions describing the half rev circle are given by Eqs. (20) and (21).

$$y'^2 + \left[z' + v_B \cos(\gamma)\right]^2 = v_{H\theta}^2 \tag{20}$$

$$x' = v_{Hr} - v_B \sin(\gamma) \tag{21}$$

The v_∞ sphere, expressed in the prime coordinates, is

$$x'^2 + y'^2 + z'^2 = v_\infty^2 \tag{22}$$

Solving for x′ ,y′, and z′ from Eqs. (20)-(22) gives the location of the two half-rev points of intersection. The coordinates, expressed in the un-primed variables, are given in Eqs. (23)-(25).

$$x = \left[v_{Hr} - v_B \sin(\gamma)\right]\cos(\gamma) + K \sin(\gamma) / \left[2 v_B \cos(\gamma)\right] \tag{23}$$

$$y = \pm\sqrt{4v_\infty^2 - 4\left[v_{Hr} - v_B \sin(\gamma)\right]^2 - K^2 / \left[v_B \cos(\gamma)\right]^2} \tag{24}$$

$$z = \left[v_{Hr} - v_B \sin(\gamma)\right]\sin(\gamma) - K / \left(2 v_B\right) \tag{25}$$

where,

$$K = 2 v_{Hr} v_B \sin(\gamma) + v_B^2 \left[1 - 2\sin^2(\gamma)\right] - v_{H\theta}^2 - v_{Hr}^2 + v_\infty^2$$

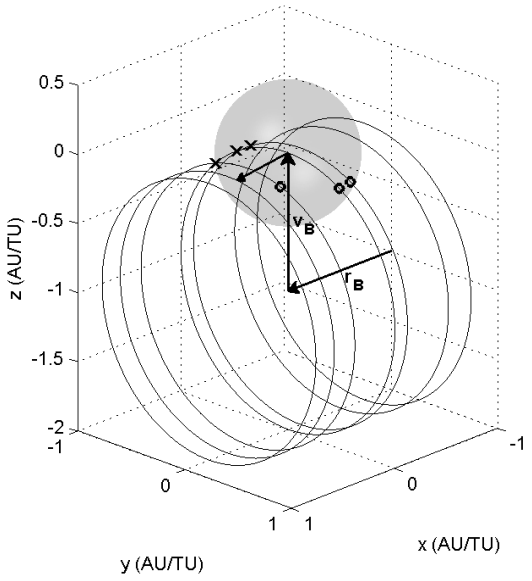

Figure 13: Half-rev velocity diagram, *M*=3.5

Continuing with the example, it is clear from Figure 6 that a time of flight of 3.5 periods yields seven corresponding solutions for semi-major axis. Thus, for this one time of flight, there are seven half-rev circles. All seven are illustrated in Figure 13. The circles form a tube-like structure with a radius, $v_{H\theta}$, and centerline, $\mathbf{r}_B$. Eq. (19) indicates that $v_{H\theta}$ is not a function of a or TOF. Therefore, the diameter of the tube is a constant for a specified μ, r_1, and r_2. For this example, it is clear that only three out of the seven circles intersect with the v_∞ =0.5 AU/TU sphere. For an intersection to exist, the y coordinate given in Eq. (24) must be non-imaginary.

Flyby Diagrams Containing All Half and Full-rev Solutions

While Figure 10 and Figure 13 illustrate the full-rev circles and half-rev points of intersection for times of flight of 4 and 3.5 celestial body periods respectively, Figure 14 includes the intersection locations for all half and full rev-return trajectories with times of flight of $n/2$ celestial body periods, where n=1→12. The full-rev spheres from Figure 10 and the half-rev circles from Figure 13 are not included. It is a projection view of the v_∞ sphere along the y axis, thus the full-rev circles appear as horizontal lines and each set of the two half-rev points appear as an 'x' underneath an 'o.' The labels along the top and to the right of the plot correspond with specific half-rev points and full-rev circles respectively. These numbers indicate the M revolutions that the celestial body will complete before the half or full-rev free-return is completed. For example, the nine 4's on the right side of the plot label the same nine full-rev circles as seen in Figure 10, and the three sets of half-rev points from Figure 13 are labeled above with a 3.5.

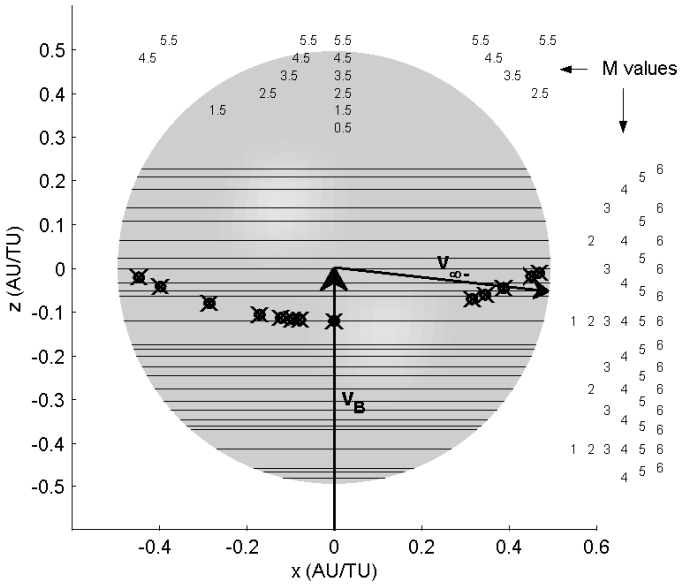

Figure 14: Potential half and full-rev locations, $|\mathbf{v}_\infty|$=0.5 AU/TU

Note that one of the half-rev point sets and several of the full-rev circles have multiple labels. This is only true in the zero-point patched conic model. Using a more realistic model, a point on the velocity diagram can't yield a true free-return trajectory if there is an intermediate encounter. Of course, in the real solar system, the radius of a planet's sphere of influence is non-zero, thus it is impossible to perform a flyby with a turning angle of zero. Consequently, $\mathbf{v}_\infty$ must rotate during a flyby. Technically, two consecutive half-rev returns on the same set of half-rev points are only possible in the realistic system if they are patched with a feasible flyby that rotates $\mathbf{v}_\infty$ from an 'x' to an 'o' or vice versa. Consecutive full-rev returns on the same full-rev circle are only possible if they are patched with feasible flybys and $\mathbf{v}_{\infty-} \neq \mathbf{v}_{\infty+}$. For the purposes of this study, the zero-point patched conic model assumptions hold. However, when transitioning solutions from this simple model to a more realistic one, the comments above should be considered.

In this example, the celestial body is in a non-inclined, circular orbit. Thus, if a spacecraft leaves the body on an inclined circular orbit in the zero-point patched conic model, it will re-encounter the body every ½ revolution. This is why the middle x/o set is labeled with each half-year. Of course, this set also lies on the full-rev circle that corresponds to the celestial body's semi-major axis.

For any value of v_∞, a velocity diagram similar to Figure 14 can be generated using Eqs. (15)-(17) and (23)-(25). This map contains all possible locations for $\mathbf{v}_{\infty+}$ such that the spacecraft will return ballistically after the body completes M revolutions of the primary. Clearly more full-rev circles and sets of half-rev points exist for larger v_∞ spheres. Examining the figures with velocity diagrams, the radius of the v_∞ spheres used for these examples is half the magnitude of the celestial body's circular velocity. This value was exaggerated intentionally for graphical purposes. Typically it is more desirable to have significantly lower hyperbolic energy levels, thus the radius for a more realistic v_∞ sphere may only be one-

quarter to one-half of the size shown in Figure 14, hence reducing the number of potential locations for full and half-rev free-returns. An example of a diagram with a more realistic v_∞ value is shown in Figure 15.

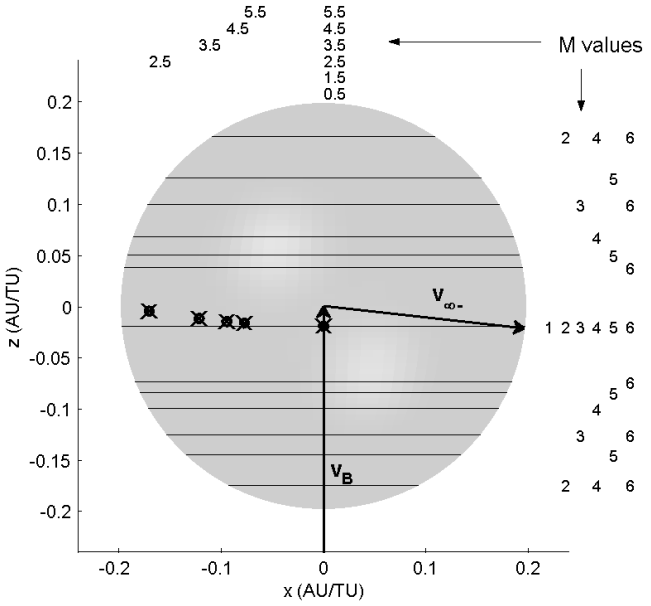

Figure 15: Potential half and full-rev locations, $|\mathbf{v}_\infty|$=0.2 AU/TU

CYCLER APPLICATIONS

Applications for generalized half and full-rev free returns include any flyby missions that require consecutive encounters with the same body. In particular, cycler missions are excellent applications because free-returns orbits are often required to satisfy the periodic time constraints.[4,10,11] For an orbit to be repeatable with respect to multiple celestial bodies, the period must be commensurate with the synodic period of the bodies. Half and full-rev free returns can be used to loiter at a body without a powered maneuver until the timing is right to begin a new cycle. This method has been successful in finding Earth-Mars cycler orbits using half and full-rev returns limited to π and 2π transfers respectively.[9,10,11] The analysis given here generalizes these terms to include $n\pi$ transfers, which significantly expands the solution space when searching for ballistic cyclers.

Reference 11 lists many ballistic and near-ballistic Earth-Mars cyclers using Earth free-return orbits. Generic returns or non-$n\pi$ transfers are patched together with π and 2π transfers such that the total cycler period is an integer multiple of the synodic period. The times of flight for the transfers were also limited to a half and full year respectively. Many of the solutions require multiple consecutive 1π and 2π transfers that each must be patched with an Earth flyby. In many cases, several of the flybys become unnecessary if the $n\pi$ transfers are considered. The first four entries in Table 2 illustrate a few favorable examples. Take *Cycler 4-11-1-10* as an example. The first number, *4*, indicates it is a four synodic period cycler, and the second number, *11*, indicates that the cycler must loiter at the Earth for eleven half-years before re-initiating the next cycle. In the method outlined in Ref 11, the optimized solution is to perform four one-year transfers with three half-year transfers in the middle, all patched by Earth flybys.

Alternatively, using the generalized definition for a half-rev transfer outlined in this paper, the seven free-return trajectories can be replaced with one 5.5-year half-rev return. Although the required turning angle increases to 107°, it still requires a flyby altitude above 200 km. Because the half-rev loitering orbit is not used for the Earth-Mars transfer, the energy characteristics of the cycler remain the same. On the contrary, the last two entries in Table 2 use three-year full-rev transfers in the ecliptic plane for the Earth-Mars transfer legs. Thus, the v_∞'s at Mars are different, in these cases significantly better, from the similar cyclers reported in Ref 11. *Cycler 4-13-1-6* has a 40% decrease in v_∞ at Mars while increasing the transit time by only 3 days. *Cycler 4-11-1-6* did not come close to Mars using the methods described in Ref. 11, thus it was not reported. However, using the general $n\pi$ transfers, a very attractive solution was found with a short transit time and low terminal speeds.

Table 2: Examples of improved solutions to previously documented Earth-Mars cyclers

Cycler	previous/ new	v_∞ Earth (km/s)	v_∞ Mars (km/s)	Earth↔Mars Transit time (days)	Sequence of *n* half-year transfers patched by flybys	Turning Angle for 200 km alt. flyby (deg)	Max Turning Angle Req. (deg)
[a]*Cycler 2-5-1-3*	previous	7.8	9.9	94	2-1-2	60	54
	new	7.8	9.9	94	**5**	60	**61**
[a]*Cycler 3-5-1-13*	previous	5.4	9.2	115	2-1-2	84	73
	new	5.4	9.2	115	**5**	84	**69**
[a]*Cycler 3-9-1-7*	previous	5.4	9.2	116	2-2-1-2-2	84	72
	new	5.4	9.2	116	**9**	84	**82**
[a]*Cycler 4-11-1-10*	previous	3.6	4.7	195	2-2-1-1-1-2-2	111	70
	new	3.6	4.7	195	**11**	111	**107**
[a]*Cycler 4-13-1-6*	previous	5.5	9.3	137	2 -2-2-1-2-2-2	84	72
	new	5.5	5.6	140	**4**-1-2-**6**	84	**79**
[b]*Cycler 4-11-1-6*	previous	-	-	-	-	-	-
	new	**3.8**	**4.8**	**168**	**2-6-2-1**	**108**	**87**

[a]Solutions documented in Ref. 11, [b]Solution found using methods outlined in Ref. 11 does not reach Mars.

A full understanding of Table 2 requires a thorough reading of Ref. 11. However, the purpose of this section is not to detail the origin of Table 2, but rather to illustrate an example application for the diagrams similar to Figure 14 and Figure 15. A future study will expand on the examples above, and give a detailed procedure to apply the methods presented in this paper to the search for cycler orbits.

CONCLUSIONS

Noting that several recent studies found practical applications for free-returns that included 1π and 2π transfers for the spacecraft and the planet, it was observed that much could be gained if the idea were generalized to include $n\pi$ transfers. The semi-major axis values for the even $n\pi$ free-return transfers, or full-rev returns, are derived both with a simple approach and taking the limit as $\mathbf{r}_1$ approaches $\mathbf{r}_2$ in Lambert's problem. Several interesting properties of the Lambert solutions are noted including the obviously impractical rectilinear ellipse solution. The semi-major axis values for the odd $n\pi$ free-return transfers, or half-rev returns, can only be found using Lambert's Equation because the times of flight are not integer multiples of orbital periods. The procedure to find these values is discussed in detail.

In velocity space, all solutions for a given half-rev return are shown to lie on a set of constant-diameter circles forming a tube, while all solutions for a given full-rev return are shown to lie on multiple concentric spheres. Intersections of these lines and surfaces with the flyby sphere of constant v_∞ identifies the half-rev points of intersection and the full-rev circles of intersection that lead to half and full-rev returns

following a flyby. The equations for all lines and points of intersection are derived, and two sample diagrams with all the feasible solutions are generated.

When including the possibility of multiple body and spacecraft revolutions, the final result is the common three-dimensional v_∞ sphere with a surface marked by multiple full-rev circles and multiple sets of two half-rev points. This resulting diagram, shows all locations following an un-powered gravity-assisted flyby, such that the spacecraft and body will re-encounter after the body makes $n/2$ revolutions of the primary. The generation of such a diagram is straight-forward, based on the geometry of the celestial body's orbit and the hyperbolic energy of the spacecraft. These diagrams are useful mission design tools for any application requiring consecutive flybys of the same body.

Although a detailed analysis of applying the $n\pi$ transfers to finding interplanetary cyclers is left to future work, this paper presents several samples of new and/or improved Earth-Mars cyclers that include the generalized half and full-rev free-returns. An effort is currently underway to find and catalog other idealized Earth-Mars cyclers using the presently described solutions. In addition, a parameter optimization system, specifically applied to finding ballistic cyclers using an accurate solar system model, is under development.

ACKNOWLEDGEMENTS

This work was performed at the University of Texas at Austin supported in part by NASA contract NGT5-141. A special thanks is owed to NASA's Goddard Space Flight Center for providing a Graduate Student Researchers Program Fellowship. I also am grateful to Troy McConaghy of Purdue University for his assistance with the three-dimensional visualization.

REFERENCES

[1] Patel, M. R., Longuski, J., M., Sims, Jon A., "Mars Free Return Trajectories," *Journal of Spacecraft and Rockets*, Vol. 35, No. 3, 1998, pp. 350-354.
[2] Miele, A., Wang, T., Mancuso, S., "Optimal Free-Return Trajectories for Moon Missions and Mars Missions," *Journal of the Astronautical Sciences*, Vol. 48, April-Sept., 2000, pp. 183-206.
[3] Wolf, A. A., "Free-Return Trajectories for Mars Missions," AAS Paper 91-123, Feb. 1991.
[4] Hollister, W. M., "Periodic Orbits for Interplanetary Flight," *Journal of Spacecraft and Rockets*, Vol. 6, No. 4, 1969, pp. 366-369.
[5] Uphoff, C. W., "The Art and Science of Lunar Gravity Assist," AAS Paper 89-170, April, 1979.
[6] Uphoff, C., Crouch, M. A., "Lunar Cycler Orbits with Alternating Semi-Monthly Transfer Windows," *Journal of the Astronautical Sciences*, Vol. 41, No. 2, 1993, pp. 189-205.
[7] Uphoff, C., Roberts, P. H., Friedman, L. D., "Orbit Design Concepts for Jupiter Orbiter Missions," *Journal of Spacecraft and Rockets*, Vol. 13, No. 6, 1976, pp. 348-355.
[8] Menning, M. D., "Freefall Periodic Orbits Connecting Earth and Venus," M.S. Thesis, Massachusetts Institute of Technology, 1968.
[9] Rall, C. S., "Freefall Periodic Orbits Connecting Earth and Mars," Ph.D. Thesis, Massachusetts Institute of Technology, 1969.
[10] Byrnes, D. V., McConaghy, T. T., Longuski, J. M., "Analysis of Various Two Synodic Period Earth-Mars Cycler Trajectories," AAS Paper 2002-4423, Aug. 2002.
[11] Russell, R., Ocampo, C., "A Systematic Approach for Constructing Earth-Mars Cyclers Using Direct Return Trajectories," AAS Paper 03-145, Feb. 2003. (Accepted to *Journal of Guidance, Control, and Dynamics,* July 2003)
[12] Prussing, J. E., Conway, B. A., *Orbital Mechanics*, Oxford University Press, New York, 1993. pp.63-80.
[13] Battin, R. H., *An Introduction to the Mathematics and Methods of Astrodynamics, Revised Edition*, American Institute of Aeronautics and Astronautics, Inc., Reston, VA, 1999, pg. 241.